GEOCHRONOMETRIA 52 (2025) 200792
DOI 10.20858/geochr/200792

Available online at https://www.geochronometria.com/

# TESTING TM-OSL ON DIFFERENT QUARTZ SAMPLES TO ILLUSTRATE THE ADVANTAGES OF THE TECHNIQUE

**PIOTR PALCZEWSKI, MAGDALENA BIERNACKA and ALICJA CHRUŚCIŃSKA**

*Institute of Physics, Faculty of Physics, Astronomy and Informatics, Nicolaus Copernicus University in Toruń, ul. Grudziądzka 5, 87-100 Toruń, Poland*

Received 16 May 2024 Accepted 4 February 2025

**Abstract**
The importance of the fast decaying signal of quartz for dating sediments is confirmed by years of research. In OSL dating, the single-aliquot regenerative-dose (SAR) protocol is applied to estimate age using quartz. The OSL signal measured in this protocol consists of components with different properties, particularly with different susceptibility to bleaching in sunlight. It is known how complicated it is to extract the fast decaying signal from other overlapping signals when blue light is used for stimulation. Decomposing OSL curves into components is unsuitable for dating purposes due to the challenges involved in handling many OSL curves for age estimation and obtaining consistent results across these curves. An OSL measurement method based on optical stimulation while the sample is heated, so-called thermally modulated OSL (TM-OSL), was recently implemented in the SAR protocol. Instead of the blue light (470 nm) typical in SAR (hereinafter referred to as SAR BLSL), red light (620 nm) is used for optical stimulation. In the protocol with TM-OSL measurement, the fast component is isolated and used for the OSL age determination. The advantage of this approach for a set of samples selected from various depositional environments is presented. The equivalent dose for the same samples was also determined using the SAR protocol that involved red light stimulation (620 nm, SAR RLSL) at an elevated temperature (230°C). The obtained results by the protocols using red light (SAR TM-OSL and SAR RLSL) are compared with the ones determined using the SAR BLSL protocol. Using TM-OSL in the SAR protocol leads to more precise dating results. The shape of the TM-OSL curve for the fast OSL component in quartz allows to identify in the TM-OSL a contribution from a signal of another origin. It prevents age underestimation by excluding from calculations the share of OSL components, which can be less stable.

**Keywords**
quartz, luminescence dating, SAR TM-OSL protocol, thermally modulated OSL

## 1. Introduction

One of the primary requirements for sediment samples in OSL dating is that the signal used for age determination is fully reset before the mineral grain deposition in the sediment layer (Huntley *et al.*, 1985, Aitken, 1998). The SAR protocol, which uses the continuous wave OSL (CW-OSL) stimulation method, widely exploited for determining the equivalent dose of quartz grains is assumed to use the OSL component (the so-called fast component) originating from traps that are the fastest emptying by light (Bailey *et al.*, 1997; Murray and Roberts, 1998; Murray and Wintle, 1998, 2000, 2003; Wintle and Murray, 1998, 1999, 2000). Just the initial fragment of the OSL decay curve measured in the protocol is used to determine the age. This is not only because of a concern that the slower signal components may not be bleached sufficiently in nature but also because of the differences in thermal stability (Jain *et al.*, 2003) and the growth curve of the individual OSL components (Singarayer and Bailey, 2003). Thus, sensitivity to optical bleaching, thermal stability, and dose-response curve, should be well-defined for any signal before dating. These properties are not unequivocally defined for the OSL signal, which is the sum of many components, mainly

Corresponding author: A. Chruścińska
e-mail: alicja@fizyka.umk.pl

ISSN 1897-1695 (online), 1733-8387 (print)

due to the different contributions of individual components in the signal of different samples. An attempt to decompose the OSL signal measured in the SAR protocol into individual components to select the fast component, could be time consuming. Various attempts have been made to develop methods for determining age using the isolated fast component from measurements in the SAR protocol, but they have found a rather limited application (Singarayer and Bailey, 2004; Li and Li, 2006; Fan *et al.*, 2009; Cunningham and Wallinga, 2009, 2010; Bailey, 2010, Durcan and Duller, 2011). Therefore, a routinely applicable method of isolating the signal from the fast component at the measurement stage is an encouraging option.

The trap parameter that governs the process of emptying traps in OSL measurements is the optical cross-section (OCS, σ, $cm^2$). It determines, together with the photon flux density ($\phi$ $cm^{-2}s^{-1}$), the probability of releasing electrons from the trap equal to $\phi\sigma$. In the simplest case, the OCS is described by the formula (Noras, 1980):

$$\sigma(h\nu) = \frac{C\kappa}{\nu\sqrt{\pi}} \int_0^{\infty} x^{\frac{1}{2}} \exp\left\{ -\kappa^2 \left[ x - \left( h\nu - E_0 \right) \right]^2 \right\} dx \quad (1)$$

$$\kappa = \left[ 2S(\hbar\omega)^2 \coth\left( \frac{\hbar\omega}{2kT} \right) \right]^{-\frac{1}{2}}, \quad (2)$$

where $h\nu$ is the stimulation energy and $x$ is a bound variable with the dimension of energy. $E_0$ is related to the thermal depth of the trap $E_T$ by the expression: $E_0 = E_T + S\hbar\omega$. The factor $S\hbar\omega$ in the simple model of optical band shape is a measure of electron-phonon coupling strength (Bourgoin and Lannoo, 1983; Skuja, 2000). The scaling constant $C$ has the dimension $cm^2s^{-1}eV^{-1/2}$ and is close to one. While $E_T$ ,$S$ and $\hbar\omega$ are parameters dependent solely on the trap, OCS is a parameter dependent also on the experimental conditions - on the energy of the photon used for stimulation (stimulation energy) and the temperature. Therefore, one can use these factors to regulate the optical stimulation so that certain traps are emptied more efficiently than others.

The thermally modulated OSL (TM-OSL) method was invented to separate the individual OSL components better (Chruścińska and Kijek, 2016) and successfully used to separate the fast component experimentally (Chruścińska and Szramowski, 2018a, 2018b). It exploits the dynamic dependence of the OCS on the temperature in the range of stimulation energies below the ionization threshold of a trap. This allows the obtaining of the OSL curve as a characteristic peak when measurement parameters: the stimulation energy, the heating rate and the photon flux density are appropriately selected. Then traps are optically emptied at sufficiently low temperatures where their thermal emptying does not occur.

It has been shown that a wavelength of 620 nm is favourable to stimulate the fast component (Chruścińska and Szramowski, 2018a, 2018b; Schmidt *et al.*, 2022). This is in agreement with the earlier reports that applying the lower stimulation energies allows for better isolating of the fast component (Singarayer and Bailey, 2003; Bailey, 2010; Bailey *et al.*, 2011). It was also shown that traps which have the next largest OCS (being the source of the medium component) are emptied efficiently after shortening the stimulation wavelength by approximately 100 nm (Palczewski and Chruścińska, 2019; Schmidt *et al.*, 2022). It means that the fast component, when measured with the stimulation wavelength of 620 nm, is well separated from the medium component.

The origin and, first of all, the stability of the medium component are not as well recognized as in the case of the fast component, and there are inconsistent reports about it in the literature. Smith and Rhodes (1994) showed that the two OSL components (fast and medium) constitute the early part of the quartz OSL signal. It was early noticed that they have different thermal stability (Bulur *et al.*, 2000). While the latter seems to be established for the fast component, one cannot state the same about the medium component of the OSL in quartz. Several earlier works (Singarayer and Bailey, 2003; Jain *et al.*, 2003; Kitis *et al.*, 2007) proved that the medium component is more stable at higher temperatures than the fast component. Then a few reports appeared showing a much lower thermal stability of the medium component (Li and Li, 2006; Steffen, *et al.*, 2009; Tamura *et al.*, 2015). (Wang *et al.*, 2015; Peng and Wang, 2020) suggested that the medium component is not a separate trap but results from the thermal release of electrons caught during optical stimulation, contributing to the TL peak at 170°C. These photo-transferred electrons primarily originate from the trap responsible for the fast component (TL peak at 325°C). However, the studies of LM-OSL correlated with TM-OSL (Schmidt *et al.*, 2022, Fig. 9) show that a separate trap is responsible for the medium OSL component in quartz – visible as a separate LM-OSL and TM-OSL component. Due to the lack of certainty about the origin of the medium component, the possibility of excluding the contribution of a medium component to the signal used for dating is a great advantage of using 620 nm.

Recently, a modified SAR procedure has been proposed. It is called SAR TM-OSL because it uses the TM-OSL method for OSL measurement instead of the CW-OSL method (Chruścińska *et al.*, 2021). In SAR TM-OSL, the TM-OSL measurement with red light stimulation is carried out during heating from 40°C to 120°C, instead of the usual blue (or green) light stimulated CW-OSL measurement at a constant temperature at 125°C. The resetting of the OSL signal is done during the stimulation with blue light in the temperature range from 120°C to 200°C. The details of the new protocol are described in **Section 2**. Previously Chruścińska *et al.* (2021) showed on a limited number of samples that the new protocol has advantages over the old one in several ways. It resulted in better recycling ratios. It also makes it possible to reject aliquots characterized by an undesirable shape of the TM-OSL signal at the stage of measuring the natural signal. For the

previously tested samples, a promising reduction in the uncertainty of the equivalent dose (ED) estimation was also demonstrated. The time consumption of the new protocol is not much greater than that of the one used so far (the duration of one new protocol cycle, excluding the irradiation and cooling of the heating strip, is approximately 30% longer than that of the standard protocol). Moreover, it is possible to shorten the duration of the SAR TM-OSL procedure significantly when a more powerful light source, i.e. a higher photon flux density, is used for stimulation. Due to the properties of TM-OSL measurement, one may then increase the heating rate by the same factor without changing the position of the TM-OSL maximum (Chruścińska and Szramowski, 2018a). Faster heating makes the TM-OSL readout time shorter.

The presented study intends to reopen a discussion on the pertinence of using blue or green light for optical stimulation in SAR protocol when the high-intensity signal of the fast OSL component can be separated from other components using a much longer wavelength. Such a possibility has been reported before (Singarayer and Bailey, 2004; Fan *et al.*, 2009; Bailey, 2010). In earlier works, authors used IR diodes for stimulation, which made the recorded OSL signal of low intensity and the measurement time impractically long. However, they irrefutably demonstrated the possibility of isolating the fast component from the others. The weaknesses of IR stimulation have recently been overcome. It has been shown that one can also achieve similarly effective isolation using red light during linear heating of a sample with satisfying OSL intensity and reading speed simultaneously.

One of the prerequisites for using photons with a high energy is the belief that higher stimulation energy corresponds to a greater probability of optically releasing the charge carrier from traps. The higher probability means the higher OSL signal and the better precision of the measurement. Based on the dependence of the OCS on the stimulation energy resulting from the simplest model of trap ionization taking into account the participation of crystal lattice vibrations (**Eqs. 1–2**), the above belief can be questioned. After a dynamic increase for the stimulation energies below and close to the optical trap depth, the OCS value increases much slower for higher energies and finally stabilizes (Chruścińska and Palczewski, 2020, Fig. 4 and 5). Such a nature of the OCS dependency on stimulation energy means that the use of higher stimulation energy may only slightly increase the OCS of the shallower trap, e.g. fast OSL component in the case of dating, while significantly increasing the OCS value of optically deeper traps. In this way, one can enhance the slow-decaying trap contribution in the overall OSL signal. The latter weakens the assumption that the SAR protocol uses mainly the fast component signal for age determination. The problem is all the greater, the bigger the share of the slower OSL components in the total OSL signal of quartz grains under investigation.

The presented research aims to compare the recently proposed protocol using the TM-OSL method with the results of the commonly used SAR protocol for a larger group of samples from different depositional environments and demonstrate that one can obtain higher precision of the equivalent dose measurement.

## 2. Experimental details

### 2.1 Sample origin

The investigation was carried out for a series of quartz samples separated from sediments of different types and ages originating from various places in Poland (**Table 1**). The samples were selected based on the results obtained from ED measurements made with the use of SAR protocol. The set of samples includes young sediments with a natural dose below 20 Gy, samples with a dose from 30 - 100 Gy and two samples with EDs close to the range of OSL signal saturation. The selection was made to include, first of all, samples with a significant proportion of slower components (samples 183, 186, 275), which was observed during SAR BLSL measurements, and samples with high relative uncertainty of ED obtained by SAR BLSL protocol (186, 183, 211, 275, 263). The younger samples (284, 285, 188) were tested to check the quality of the SAR TM-OSL results in the case of predicted low natural signals.

**Table 1.** *Sediment samples used in the investigation and their origin. The age was determined using the SAR BLSL protocol.*

| Sample | ED (SAR BLSL), Gy | Age (SAR BLSL), ka | Type of sediments | Origin |
|---|---|---|---|---|
| **284** | 10.9 ± 1.0 | 14.7 ± 2.6 | aeolian | Upper Silesia |
| **285** | 14.7 ± 1.5 | 15.0 ± 2.2 | aeolian | Upper Silesia |
| **188** | 20.2 ± 3.1 | 19.6 ± 8.4 | aeolian | Upper Silesia |
| **183** | 34 ± 12 | 31 ± 11 | glacial | Pomeranian Lake District |
| **275** | 74 ± 31 | 88 ± 30 | fluvial | Upper Silesia |
| **263** | 80 ± 28 | 171 ± 53 | fluvial | Western Polesie |
| **186** | 271 ± 90 | close to saturation | fluvioglacial | Lesser Poland Upland |
| **211** | 255 ± 96 | close to saturation | limnoglacial/kame* | Polish Plain |

**Kame is a glacial landform shaped by meltwater from the glacier, a few to several meters high and several hundred meters in diameter, with the shape of a cone or a truncated cone, mostly built with sand, silt or gravel.*

One part of the samples is aeolian, and the other fluvial sediments. They include samples with the ages estimated by the OSL method ranging from several thousand to around two hundred thousand years (samples 186 and 211). The latter samples, whose estimated OSL age is above the currently accepted time range of the OSL method with the use of quartz (Chapot *et al.*, 2012; Timar-Gabor and Wintle, 2013; Timar-Gabor *et al.*, 2015; Peng *et al.*, 2022), were selected to check the difference between SAR and SAR TM-OSL results in the region of OSL signal saturation.

### 2.2 Sample preparation

All samples were prepared using procedures common in luminescence dating, including sieving, separation in heavy liquids and etching with 40% HF. Quartz grains size 100–150 μm were deposited on stainless steel discs using Silkospray and a mask that ensures a 6 mm aliquot diameter.

### 2.3 Equipment

The SAR protocol measurements were made using the Risø TL/OSL System TL-DA-20 and its standard blue diode OSL unit. Photomultiplier EMI 9235QB equipped with the 7.5 mm Hoya U-340 filter was used for luminescence detection. All SAR TM-OSL and SAR RLSL measurements were carried out using a Risø TL/OSL-DA-12 (after a refurbishment) equipped with an EMI 9235QB15 photomultiplier, the combination of a 2 mm Hoya U340 and 2 mm Chroma 79-340 bandpass filters. An external unit for the optical stimulation allowed the stimulation with two LED modules made of single high-power LEDs (3 W, Bridgelux, Inc.). The maxima of their spectral bands are 620 nm and 470 nm. The LED modules are integrated with the Risø reader via a dedicated optical adapter, mounted instead of the earlier used halogen lamp. In both readers, all measurements were conducted in the Ar atmosphere. The $^{90}Sr/^{90}Y$ β sources delivering dose rates of about $31.2 \pm 0.9$ mGy·s$^{-1}$ or $97.6 \pm 4.7$ mGy·s$^{-1}$ were applied for the irradiation of samples in the old Risø TL/OSL-DA-12) and the new reader (Risø TL/OSL System TL-DA-20), respectively.

### 2.4 Protocols

When the red light is enough to stimulate the fast component in quartz, the question arises whether one can use the red light instead of blue light in a regular SAR measurement using the CW-OSL method and thus determine the age based on the separated fast OSL component.

To answer that question, a series of tests of the SAR protocol was carried out by replacing the blue LEDs with red ones for the first 25 seconds of measuring the signal from the regenerative dose and the test dose. After 25 seconds, the stimulation was continued with blue LEDs for the 40s. Tests were performed on quartz samples supplied by Risø for source calibration (Hansen *et al.*, 2015) and consisted in performing dose recovery tests for various stimulation temperatures. The preheat temperature was taken from the SAR TM-OSL, as it previously proved to be the best when the fast component was stimulated with red light. The temperature of 230°C was the lowest, for which acceptable results of the recycling and recuperation tests were obtained, and of course, the correct reproduction of the initially delivered dose. The lowest temperature was chosen to minimize changes in sample sensitivity.

The protocol established this way, which we will call SAR RLSL, was also used to determine the equivalent dose for the investigated sediment samples. We compare these results with the results obtained for the other two methods. **Table 2** presents the subsequent steps of three protocols examined in the study together with experimental parameters applied in each of them. The new protocols, just like the SAR BLSL protocol, provide steps to correct changes in the sample sensitivity during measurements (steps 4–6) and the entire cycle repetitions to perform the recycling (repetition for regenerative dose $D_1$) and the recuperation tests (repetition for regenerative dose equal to zero).

The regenerative doses in the SAR TM-OSL and SAR RLSL protocols were selected to cover a range of doses around the EDs obtained in the SAR BLSL protocol. The selection of the preheat temperature in the SAR BLSL protocol equal to 240°C was verified by the dose-recovery tests. The preheat temperature in the SAR TM-OSL protocol (260°C) was established at the stage of developing a new protocol. So far, the recycling and recuperation test results and the dose-recovery tests for the samples investigated with this protocol confirm the correctness of this choice for individual samples. The results of the tests are presented in **Table 4**.

Steps 3 and 6 in SAR TM-OSL and in SAR RLSL protocols, which mainly make the difference between these protocols and the OSL SAR, require more clarification. During these steps in SAR TM-OSL protocol, the stimulation with light wavelength 620 nm is carried out from 40°C to 120°C and the subsequent bleaching of the fast OSL component by the stimulation with blue diodes conducted during the continued heating up to 200°C. Steps 3 and 6 in protocol SAR RLSL include the stimulation with the wavelength of 620 nm for the first 25 s. Subsequently, the bleaching of the signal is continued by stimulation with 470 nm for the next 40 seconds. Both kinds of stimulation are carried out at a constant temperature of 230°C.

### 2.5 Experimental data processing

The values of the $L_x$ and $T_x$ signals needed for the growth curves construction in the SAR BLSL procedure were determined in a standard way. One took into account the sum of the counts for the first five measurement channels (the first 0.8 s) and, as the background, the counts from the last ten channels (so-called late background). Due to the lack of adaptation of the Analyst software for TM-OSL measurements, determining Lx and Tx in the SAR TM-OSL procedure requires some effort. It concerns mainly the way

**Table 2.** *Steps of the SAR BLSL, SAR TM-OSL and SAR RLSL protocols. The photon flux densities in the TM-OSL and SAR RLSL protocols were $5.3 \cdot 10^{17}$ cm$^{-2}$s$^{-1}$ for stimulation with 620 nm and $5.5 \cdot 10^{16}$ cm$^{-2}$s$^{-1}$ for 470 nm.*

| Step | SAR BLSL | SAR TM-OSL | SAR RLSL |
|---|---|---|---|
| 1 | Excitation, regenerative dose $D_i$ (i = 0,1,.., n) * | Excitation, regenerative dose $D_i$ (i = 0,1,.., 5) ** | Excitation, regenerative dose $D_i$ (i = 0,1,.., 5) ** |
| 2 | Preheat for 10 s at 240°C, heating rate 5 Ks$^{-1}$ | Heating with the rate 2 Ks$^{-1}$ to 260°C | Heating with the rate 2 Ks$^{-1}$ to 260°C |
| 3 | Optical stimulation for 40 s at temperature 125°C | TM-OSL with heating rate 2 Ks$^{-1}$ to 200°C, from 40°C to 120°C stimulation with 620 nm and, next, from 120°C to 200°C stimulation with 470 nm to bleach the OSL | Stimulation at 230°C, first 25 s with 620 nm and then 40 s with 470 nm to bleach the OSL |
| 4 | Excitation, test dose | Excitation, test dose | Excitation, test dose |
| 5 | Preheat for 10 s at 240°C, heating rate 5 Ks$^{-1}$ | Heating with the rate 2 Ks$^{-1}$ to 260°C | Heating with the rate 2 Ks$^{-1}$ to 260°C |
| 6 | Optical stimulation for 40 s at temperature 125°C | TM-OSL with heating rate 2 Ks$^{-1}$ to 200°C, from 40°C to 120°C stimulation with 620 nm and, next, from 120°C to 200°C stimulation with 470 nm to bleach the OSL | Stimulation at 230°C, first 25 s with 620 nm and then 40 s with 470 nm to bleach the OSL |
| 7 | Optical stimulation for 40 s at temperature 280°C | Return to step 1 for the next cycle | Return to step 1 for the next cycle |
| 8 | Return to step 1 for the next cycle | | |

**) The number of regeneration doses for the SAR BLSL protocol was often greater than five because the protocol was used as the first, and the regenerative doses had to be adjusted to reproduce the natural signal.*

***) $D_0$ is equal to zero because the naturally excited OSL is measured during the first cycle of the SAR BLSL protocol. $D_5$ is also equal to zero because cycle 5 is reserved for the recuperation test.*

of including the background. In the SAR TM-OSL protocol, $L_x$ (and $T_x$) was the sum of the photomultiplier counts from 40 to 114°C minus the background. The temperature range of 40–120 is the range in which light with a wavelength of 620 nm is used for stimulation. The signal integration is performed to a safely lower temperature, not to add counts from the region of switching the red light to blue.

The background includes the noise of the photomultiplier, a negligible fraction of the stimulation light transmitted through the detection window filters. One should also include the steady luminescence signal related to the silicon oil used for depositing grains on discs (Vandenberghe *et al.*, 2008; Chruścińska *et al.*, 2020). The background was determined for each aliquot after the OSL bleaching with the blue light when the SAR TM-OSL procedure was finished (step 8 in the SAR TM-OSL protocol in **Table 2**). **Fig. 1** shows examples of background measured for several aliquots of sample 183. The central part of the figure shows the part of the overall signal in the temperature range from 40 to 120°C used to determine the signal background in the SAR TM-OSL protocol. The entire measurement is shown in the inset. It is worth noting the different background levels observed here. At the lowest temperatures, there is the photomultiplier self-noise. Then, in the range 40–120°C, the background is used to determine Lx and Tx, with the abovementioned components. Above 120°C, the background level is considerably higher. It is mainly related to the rest of the unbleached signal from the slowest components, the blue light transmitted through the detection filters, and the higher emission of silicone oil under blue light stimulation (Chruścińska *et al.*, 2020).

From the described background measurement, one could determine the mean of the photomultiplier counts in the range of 40–114°C. Next, this value was inserted into the first two channels of all the curves measured in the SAR TM-OSL protocol for a given aliquot. It allowed taking into account the background in the analysis performed with the help of the Analyst program. Lx was determined, as mentioned above, by subtracting from the TM-OSL signal in the range 40–114°C the background determined by the first two measurement channels.

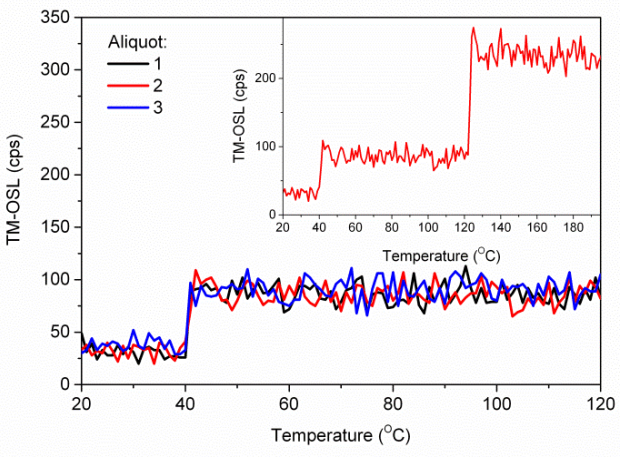


**Fig. 1.** *Examples of curves measured for each aliquot to determine the background and, finally, the Lx and Tx values in the SAR TM-OSL protocol. The inset shows the shape of the entire curve, while the central part is only the fragment used to calculate the background.*

In the SAR RLSL protocol, Lx (and Tx) was the sum of the photomultiplier counts from the first five seconds of red light stimulation. The counts from the 21st to the 25th seconds were used to estimate the background. Apart from determining Lx and Tx values and the background, the determination of EDs with the Analyst software in the red light protocols was similar to the SAR BLSL protocol.

Outcomes of the all protocols were presented in the simplest possible and raw manner by calculating only the average ED value and its corresponding standard deviation. Minimizing the impact of the statistical approach on the presented results seems to be the best way for the presentation in the case of the protocol comparison.

## 3. Results

### 3.1 Luminescence characteristic of the samples

When several samples are used to compare measurement protocols to determine the ED, it is worth looking at the differences between samples in the luminescence characteristics. They are shown in **Fig. 2** for TL and **Fig. 3** for the BLSL, TM-OSL and RLSL. TL experiments were performed after the initial short heating to 500°C. Before the TL and OSL measurement, samples were irradiated with a dose of 100 Gy. The preheat to 240°C was applied before BLSL and to 260°C in the case of the TM-OSL and RLSL readout.

First of all, it is good to notice that the thermoluminescence curves of the samples used for the comparison presented in **Fig. 2** have similar shapes. The most significant differences in the TL signal intensity occur above 300°C. This temperature range for the TL curve measured with the heating rate of 2 $Ks^{-1}$ is above the region of the TL peak related to the fast OSL component (Smith *et al.*, 1986; Spooner, 1994; Murray and Wintle, 1998; Jain *et al.*, 2003; Singarayer and Bailey, 2004). One can observe more considerable variations in the BLSL intensity (**Fig. 3**), but, like the TL, not in the shapes of the curves. The differences in the initial BLSL intensity are more evident in the inset of **Fig. 3a**. The order of the OSL initial intensities for the individual samples, as seen in the inset of **Fig. 3a**, is also reflected in TM-OSL (**Fig. 3b**) and RLSL curves (**Fig. 3c**) since the latter exhibit the intensities of the fast component. The sample 275 has the lowest intensity consistently, and samples 183, 284, and 285 are distinguished by the highest intensity. As was observed in experiments presented below in **Section 3.4**, these mutual relations of sample OSL intensities change from aliquot to aliquot. So results presented here only confirm that there are no essential differences in the TL and OSL properties of the tested samples and do not allow for deriving quantitative conclusions on the samples' signal intensity.

One should pay attention to the shape of the TM-OSL curves (**Fig. 3b**), which is preserved from sample to sample. It is not distorted in the way presented for some quartz aliquots in the previous publication concerning the SAR TM-OSL protocol, where a characteristic fast decay appeared in the initial part of the TM-OSL curve (Chruścińska *et al.*, 2021). The individual grains that were the source of disturbance of the TM-OSL curve were separated. Analysis of these grains by scanning electron microscopy with an X-ray fluorescence probe (SEM-XRF) showed that they were not quartz grains. Shapes of TM-OSL curves observed in this study, as discussed in **Section 4**, are mostly the same as those observed for similar experimental conditions in reference quartz samples tested for quartz purity (see for example Schmidt *et al.*, 2022).

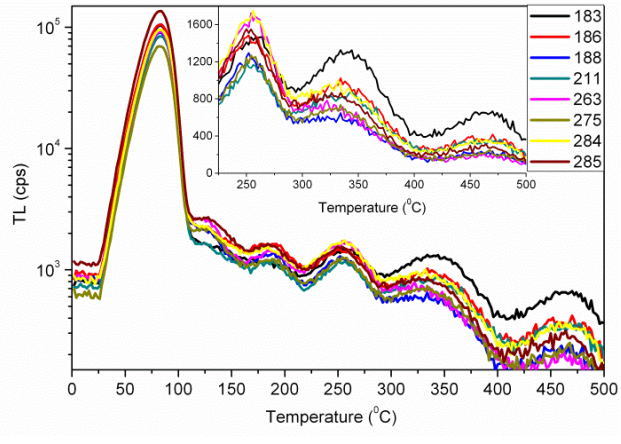


**Fig. 2.** *TL curves of the quartz samples used in the study. The measurement was done with a heating rate of 2 $Ks^{-1}$ immediately after irradiation with a dose of 100 Gy. The inset is the same plot with a linear scale of the TL-axis showing the curves in the temperature range of 200–500°C.*

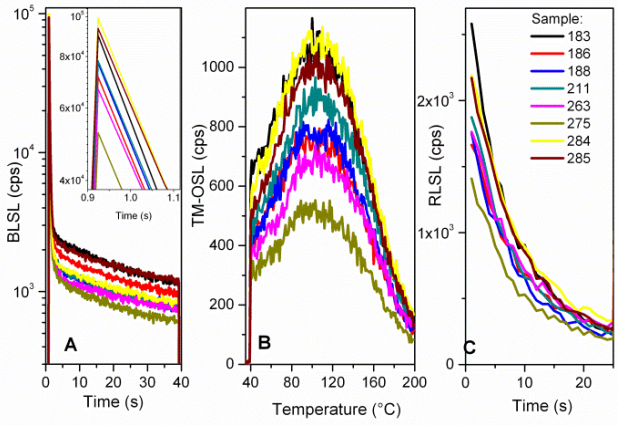


**Fig. 3.** *Luminescence obtained by the discussed methods after 100 Gy excitation: OSL with 470 nm stimulation (BLSL) at 125°C (A), TM-OSL with stimulation 620 nm, heating rate 2 $Ks^{-1}$ and the photon flux density in of $1.5 \cdot 10^{17}$ $cm^{-2}s^{-1}$ (B) and OSL with 620 nm stimulation (RLSL) at temperature 230°C (C). The inset in part A is the same plot as in the main part with a linear OSL-axis. It shows more precisely the differences in the initial intensity of the samples' OSL signal.*

### 3.2 Equivalent dose

**Table 3** contains results of ED estimation for all applied protocols. The ED values shown in the table are average values of results obtained for aliquots, which fulfilled conditions of the recycling and the recuperation tests (the recycling test result within 0.9–1.1, the recuperation test result less than 5%; Wintle and Murray, 2006). In the same column, the standard deviation (SD) values are presented to present the scatter of results for individual samples to present the scatter of results for individual samples. In the adjacent columns, "CAM ED", "OD (%)", and "Err (%)", respectively, the ED, over-dispersion and percentage error values determined using the central age model (CAM; Galbraith *et al.*, 1999) are shown. The further part of the discussion uses the results in the "mean ED/SD" column, which is the most straightforward presentation of measurement data obtained in the protocols, not subjected to any additional analysis but directly related to the result in the subsequent columns. The aliquot number used in measurements for a given sample ranged from 10 to 24 and is given in **Table 3** next to the number of aliquots that passed the tests (column "test").

In the table, the "test" column in the part for the SAR RLSL protocol stands out. For all protocols, this column shows a ratio of the number of samples that passed the recycling and the recuperation tests to the initial number of samples used in measurements. The SAR RLSL protocol for all samples except those on the saturation edge did not allow obtaining proper recycling or recuperation test results for a significant part of aliquots. For most cases, apart from the oldest samples (186, 211), no improvement in the precision of the obtained ED values was noticed compared to the results of the SAR BLSL protocol. These results indicate that the SAR RLSL protocol, although it gave positive preliminary results for the calibration quartz sample, is not suitable for use in dating. For this reason, the detailed results for this protocol will not be discussed further.

In both other protocols, SAR BLSL and SAR TM-OSL, the vast majority of samples passed recycling and recuperation tests. However, it is easy to notice the difference in the precision of the results for both protocols. The SAR TM-OSL protocol leads to much more precise ED values than the SAR BLSL protocol for all samples except samples 284 and 285. The difference in the relative uncertainties in the results of both protocols is clearly visible in **Fig. 4**. The relative uncertainties of EDs obtained in the SAR BLSL protocol for older samples (183, 275, 263, 186, 211) are within 30–40%. As mentioned above, these samples were specially selected for testing from previously dated samples precisely because their EDs obtained using SAR BLSL have significant uncertainties. Their ED percent errors (see **Table 3**) in the case of the SAR TM-OSL

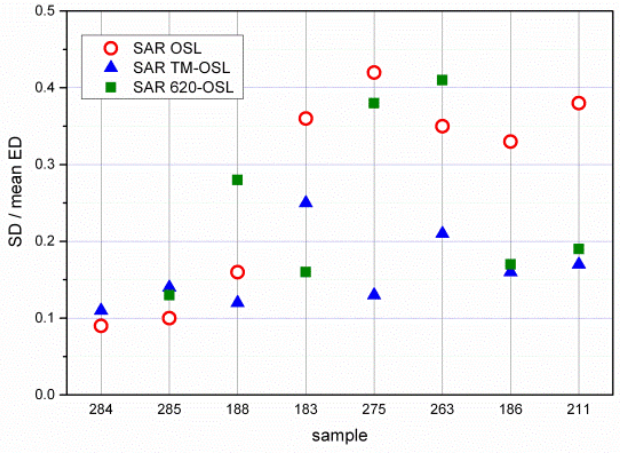


**Fig. 4.** *The ratio of the standard deviation to the mean of equivalent dose obtained with measurements made by SAR BLSL, SAR TM-OSL and SAR RLSL methods. The samples are arranged in order from the youngest (284) to the oldest (211) sample.*

**Table 3.** *Summary of measurement results using SAR BLSL, SAR TM-OSL and SAR RLOSL methods. The arithmetic means and standard deviations of ED values obtained for individual aliquots of each sample, obtained from the central age model weighted-mean ED (CAM ED), the over-dispersion (OD) of the ED, end corresponding to CAM ED per cent error (Err) are shown for SAR BLSL and TM-OSL protocols. For SAR RLSL, only the arithmetic mean values and the standard deviations are presented. Columns "tests" show the number of aliquots that have passed recuperation and recycling tests with the total number of aliquots measured.*

| Sample | SAR BLSL | | | | | SAR TM-OSL | | | | | SAR RLSL | |
|---|---|---|---|---|---|---|---|---|---|---|---|---|
| | mean ED/SD (Gy) | CAM ED (Gy) | OD (%) | Err (%) | tests | mean ED/SD (Gy) | CAM ED (Gy) | OD (%) | Err (%) | tests | mean ED/SD (Gy) | tests |
| **284** | 10.9/1.0 | 10.9±0.8 | 7 | 7.0 | 16/16 | 11.2/1.2 | 11.2±0.7 | 9 | 6.3 | 9/12 | - | 0/12 |
| **285** | 14.7/1.5 | 14.6±1.1 | 10 | 7.7 | 16/16 | 13.4/1.9 | 13.3±0.9 | 12 | 6.4 | 14/24 | 13.8/1.8 | 3/24 |
| **188** | 20.2/3.1 | 20.0±1.6 | 14 | 8.2 | 24/24 | 20.7/2.5 | 20.5±1.4 | 11 | 6.7 | 10/12 | 22.2/6.3 | 4/12 |
| **183** | 34/12 | 32.1±3.7 | 31 | 11.4 | 16/16 | 30.8/7.7 | 29.9±2.3 | 22 | 7.8 | 22/23 | 52.6/8.3 | 4/11 |
| **275** | 74/31 | 65±10 | 37 | 15.3 | 16/16 | 65.8/8.6 | 64.5±3.8 | 12 | 5.8 | 21/23 | 63/25 | 9/12 |
| **263** | 80/28 | 75±10 | 27 | 13.4 | 15/16 | 68/12 | 72.0±5.8 | 12 | 8.1 | 14/15 | 91/38 | 7/13 |
| **186** | 271/90 | 252±30 | 33 | 11.9 | 24/24 | 216/35 | 211±16 | 13 | 7.2 | 12/13 | 232/40 | 11/11 |
| **211** | 255/96 | 232±43 | 45 | 18.4 | 13/13 | 258/44 | 250±18 | 8 | 7.0 | 10/10 | 259/50 | 10/10 |

protocol are at least 10% lower (183), and in most cases 20% smaller (275, 263, 186, 211). For sample 188, the difference is less favourable for the SAR TM-OSL protocol, for which the percent error is only 5% smaller than in SAR BLSL protocol. EDs obtained for the youngest samples 284 and 285 have errors smaller when obtained in the SAR BLSL protocol, by 2% and 4%, respectively.

A better comparison of the ED values obtained by both protocols may be done by analysis of **Fig. 5** and **6**. They present the comparison of EDs obtained for individual aliquots of all the samples by SAR BLSL and SAR TM-OSL protocols. Again, ED values are shown only for aliquots that have passed the recycling and the recuperation tests. In order to present the extent of differences between the results for individual aliquots of a given sample, one added, in the graphs, the normal probability distribution curves corresponding to the mean values and the standard deviation determined from the presented results.

The results of measurements for the youngest samples can be seen on the top of **Fig. 5**. They show that taking into account the standard error of estimated ED values both protocols lead to consistent EDs. However, in the case of a low natural signal, the SAR BLSL protocol allows for better ED precision (samples 284 and 285) than SAR TM-OSL. Especially for sample 285, there are much more significant differences between the EDs obtained by the SAR TM-OSL method for individual aliquots than for the SAR BLSL results. At the same time, there is a noticeable shift in the individual ED values for SAR TM-OSL towards lower doses. In the case of sample 188, that is a bit older than samples 284 and 285, there is no difference between results of both protocols presented in **Fig. 5c**.

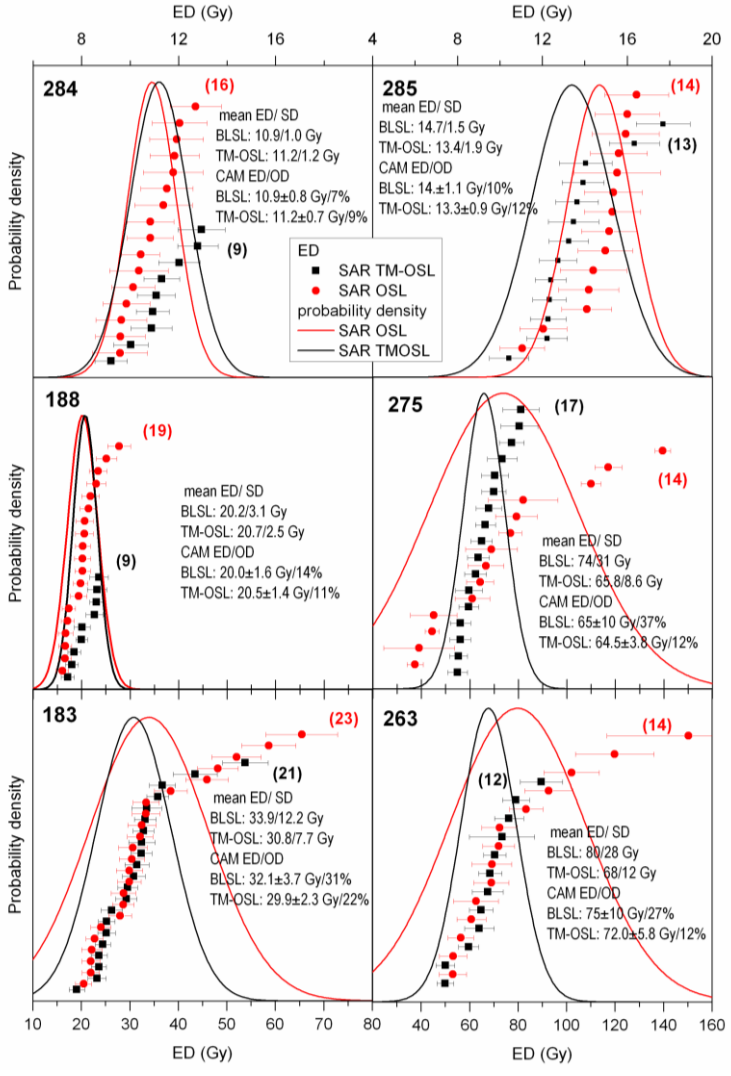


**Fig. 5.** *Mean ED values with corresponding SD and ED values determined by CAM obtained as the results of the SAR BLSL and the SAR TM-OSL protocol for six sediment samples whose OSL signal is below the saturation level. The shapes of the probability density curves are shown in order to illustrate the spread of ED values for the individual aliquots of the samples. The number of aliquots used for density calculations is given next to the individual plots.*

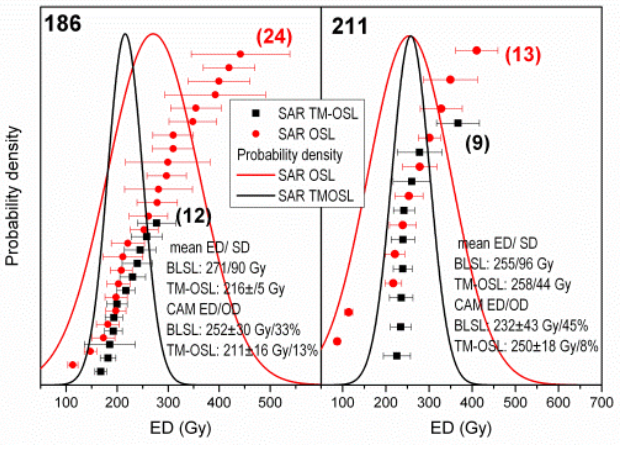


**Fig. 6.** *Mean ED values with corresponding SD and ED values determined by CAM acquired by the SAR BLSL and the SAR TM-OSL protocol for two sediment samples characterised by very high natural OSL signal laying in the range of the saturation. The shapes of the probability density curves are shown in order to illustrate the spread of ED values for the individual aliquots of the samples. The number of aliquots used for density calculations is given next to the plots.*

The parts d, e and f of **Fig. 5** present EDs obtained for aliquots of samples selected due to significant ED uncertainties as measured with SAR BLSL. These were the biggest for sample 275, and in this case, the improvement of the ED precision when using the SAR TM-OSL protocol is most noticeable. Considering the uncertainties, the EDs obtained in both protocols are consistent. Similarly, these values are compatible for samples 183 and 263. Although the reduction of ED spreads for aliquots measured by the SAR TM-OSL protocol is less spectacular here, fewer values significantly deviate from the average. For sample 263, there is a more significant difference between the mean ED values for both protocols than for the remaining samples. **Fig. 6** compares the outcomes of both protocols for samples with EDs in the saturation range. Again, the confidence intervals of the results overlap, and one can observe much lower uncertainties for SAR TM-OSL results. For sample 211, the ED mean values from both protocols agree. In contrast, the mean ED value from the SAR TM-OSL measurements for Sample 186 is approximately 20% less than that obtained from the SAR BLSL.

Summing up, as seen in **Fig. 5** and **6**, for samples selected for the investigation characterized by a wide spread of ED values obtained for individual aliquots by SAR BLSL protocol, the application of SAR TM-OSL protocol brings significantly less dispersed results (samples 183, 275, 263, 186, 211). In these cases, it is characteristic that although the confidence intervals of the determined values of ED overlap, a shift of the mean ED value towards lower doses is observed. No significant improvement in the ED precision is obtained by applying SAR TM-OSL protocol for young samples, whose EDs from SAR BLSL are not highly dispersed.

### 3.3 Sensitivity changes and tests' results

**Fig. 7** makes it possible to compare changes in the quartz sensitivity during both dating procedures. One plot in this figure presents the averaged data over all aliquots included in the ED determination for a given sample. Changes in OSL sensitivity are observed during both protocols by measuring OSL excited by the test dose applied after the natural OSL measurement and the regenerative dose-induced OSL (step 6 in **Table 2**).

The results presented in **Fig. 7** show that the SAR TM-OSL protocol leads to smaller changes in sensitivity in young samples compared to the SAR BLSL protocol. For older samples tested, the range of changes in sensitivity in both protocols are comparable, but the results for the SAR TM-OSL protocol have a smaller scatter. No correlation is observed between the relative change in sensitivity and the uncertainty of the ED value.

**Table 4** contains the arithmetic means (and their standard errors) of the tests' results; the recycling, recuperation and dose-recovery ratio (Murray and Wintle, 2000); obtained for all aliquots that passed all tests and were included in the calculation of ED obtained in SAR BLSL and SAR TM-OSL protocols. The ratio of the measured dose to the known dose applied after the bleaching of the natural signal, i.e. the dose-recovery ratio, is presented in columns 4 and 7.

As shown in **Table 4**, the dose-recovery ratios for the individual samples are for both protocols consistent within uncertainties, and all are close to one. The recycling ratios of all samples are close to one. Such was the criterion of including a sample in ED calculation. Nevertheless, the ratios for SAR TM-OSL protocol fluctuate slightly more around the mean values. Recuperation ratios for both protocols agree within uncertainties. However, a bit larger

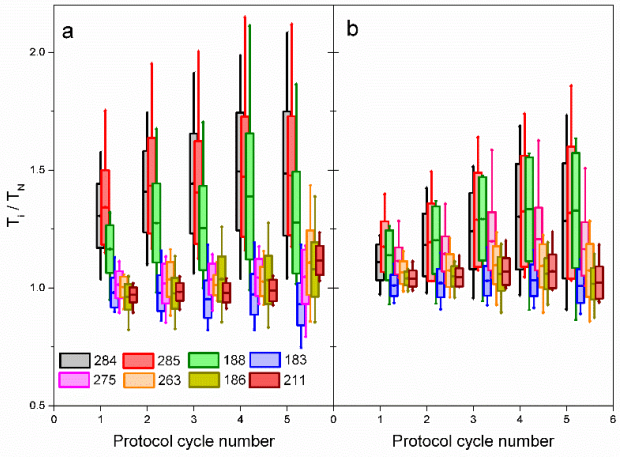


**Fig. 7.** *Sensitivity changes along the cycles of SAR BLSL (a) and SAR TM-OSL (b) protocol for all investigated samples. $T_i/T_N$, for the subsequent cycles of the protocol, is the ratio of the OSL signal measured after the test dose following the i-th regenerative dose to the OSL signal after the test dose applied after the natural signal measurement.*

**Table 4.** *Mean values of recuperation, recycling and dose-recovery tests obtained from ED measurements using SAR BLSL and SAR TM-OSL methods.*

| Sample | SAR BLSL | | | SAR TM-OSL | | |
|---|---|---|---|---|---|---|
| | Recycling | Recuperation (%) | Recovery | Recycling | Recuperation (%) | Recovery |
| **284** | 1.01 ± 0.02 | 0.89 ± 0.22 | 0.98 ± 0.02 | 1.01 ± 0.02 | 0.84 ± 0.15 | 1.00 ± 0.02 |
| **285** | 1.01 ± 0.01 | 0.68 ± 0.17 | 0.96 ± 0.02 | 1.03 ± 0.02 | 1.08 ± 0.27 | 0.97 ± 0.02 |
| **188** | 1.03 ± 0.01 | 0.46 ± 0.07 | 0.96 ± 0.02 | 1.02 ± 0.02 | 0.82 ± 0.28 | 0.96 ± 0.02 |
| **183** | 1.01 ± 0.01 | 0.26 ± 0.07 | 1.00 ± 0.02 | 1.00 ± 0.08 | 0.90 ± 0.17 | 0.99 ± 0.01 |
| **275** | 1.00 ± 0.01 | 0.45 ± 0.21 | 0.94 ± 0.01 | 1.03 ± 0.01 | 0.87 ± 0.21 | 0.97 ± 0.01 |
| **263** | 0.99 ± 0.01 | 0.50 ± 0.28 | 0.94 ± 0.02 | 1.03 ± 0.02 | 0.60 ± 0.14 | 0.99 ± 0.02 |
| **186** | 1.01 ± 0.01 | 0.25 ± 0.04 | 0.96 ± 0.04 | 1.02 ± 0.10 | 0.58 ± 0.17 | 0.96 ± 0.02 |
| **211** | 1.02 ± 0.01 | 0.22 ± 0.06 | 0.93 ± 0.02 | 1.02 ± 0.01 | 0.33 ± 0.12 | 0.95 ± 0.02 |

scatter of the ratio appears for the SAR TM-OSL protocol. Thus, summing up, no significant differences in the test results for the protocols compared were noticed.

### 3.4 The share of the fast and the medium components in the CW-OSL signal

As mentioned above, the cause of dating problems is often the participation of the components decaying slower than the fast component in the signal used to determine ED. Therefore, it is worth taking a closer look at components of the CW-OSL signal used in the SAR BLSL protocol.

**Table 5** presents the results of the CW-OSL curves' decomposition. The decomposition was performed by fitting the sum of four OSL curves of first-order kinetics to the measurement curves. Increasing the number of components did not cause significant changes in the values of the fit parameters for the fast and medium components. In fitting, one used the measurement curves obtained after 100 Gy irradiation and preheating up to 240°C. The experimental curves for aliquots with number 1, whose decomposition results appear in the **Table 5**, are presented in **Fig. 3a**. The graphical presentation of the fitting results, i.e. the first-order decay curves (simple exponential decay), their sum and the experimental curve for a selected aliquot of sample 183 and 186, is shown in **Fig. 8**.

As can be seen, all tested samples have a significant share of the medium component in the CW-OSL signal. The entire set of medium component contribution ranges from 19% to 78%. Moreover, one can observe significant differences in the contribution of this component to the total signal between the curves measured for the same sample.

One should emphasize that similarly considerable fluctuations from aliquot to an aliquot are observed for the intensity of the fast component measured by the TM-OSL method with a wavelength of 620 nm in the case of all investigated samples. **Fig. 9** presents examples of pairs of results for several tested samples. The curves are shown after subtracting the background measured after the OSL

**Table 5.** *Results of fitting the sum of four exponential decay functions to the CW-OSL curves. For each sample, results for two aliquots are presented. The table is organized to facilitate the comparison of parameters obtained for aliquots of the same sample. The parameters of fitting quality $R^2$ are given in the last lines. $t_i$ and $A_i$ ($i$ = 1, ..., 4) represent the decay time constant and the intensity of the $i$-th component, respectively.*

| | | | Sample | | | | | | | |
|---|---|---|---|---|---|---|---|---|---|---|
| component | aliquot | | 183 | 186 | 188 | 211 | 263 | 275 | 284 | 285 |
| background | 1 | $\gamma_0$ | 0.010 ± 0.001 | 0.011 ± 0.001 | 0.007 ± 0.001 | 0.007 ± 0.001 | 0.009 ± 0.001 | 0.009 ± 0.001 | 0.007 ± 0.001 | 0.010 ± 0.001 |
| | 2 | $\gamma_0$ | 0.007 ± 0.001 | 0.011 ± 0.001 | 0.005 ± 0.001 | 0.005 ± 0.001 | 0.008 ± 0.001 | 0.005 ± 0.001 | 0.012 ± 0.001 | 0.016 ± 0.001 |
| fast | 1 | $A_1$ | 0.61 ± 0.11 | 0.17 ± 0.04 | 0.28 ± 0.09 | 0.43 ± 0.05 | 0.49 ± 0.05 | 0.77 ± 0.07 | 0.62 ± 0.12 | 0.42 ± 0.06 |
| | 1 | $t_1$ (s) | 0.12 ± 0.01 | 0.07 ± 0.01 | 0.10 ± 0.01 | 0.11 ± 0.01 | 0.12 ± 0.01 | 0.14 ± 0.00 | 0.13 ± 0.01 | 0.11 ± 0.01 |
| | 2 | $A_1$ | 0.73 ± 0.06 | 0.77 ± 0.37 | 0.58 ± 0.06 | 0.68 ± 0.10 | 0.67 ± 0.09 | 0.59 ± 0.07 | 0.36 ± 0.15 | 0.45 ± 0.13 |
| | 2 | $t_1$ (s) | 0.13 ± 0.01 | 0.13 ± 0.01 | 0.11 ± 0.01 | 0.11 ± 0.01 | 0.12 ± 0.01 | 0.14 ± 0.01 | 0.10 ± 0.02 | 0.11 ± 0.01 |
| medium | 1 | $A_2$ | 0.34 ± 0.10 | 0.78 ± 0.03 | 0.69 ± 0.08 | 0.54 ± 0.05 | 0.47 ± 0.05 | 0.19 ± 0.06 | 0.35 ± 0.12 | 0.55 ± 0.06 |
| | 1 | $t_2$ (s) | 0.22 ± 0.03 | 0.19 ± 0.01 | 0.20 ± 0.01 | 0.23 ± 0.01 | 0.26 ± 0.01 | 0.29 ± 0.05 | 0.23 ± 0.02 | 0.23 ± 0.01 |
| | 2 | $A_2$ | 0.25 ± 0.06 | 0.19 ± 0.36 | 0.40 ± 0.06 | 0.68 ± 0.10 | 0.30 ± 0.09 | 0.39 ± 0.07 | 0.60 ± 0.15 | 0.51 ± 0.12 |
| | 2 | $t_2$ (s) | 0.26 ± 0.03 | 0.21 ± 0.12 | 0.20 ± 0.01 | 0.19 ± 0.01 | 0.23 ± 0.02 | 0.25 ± 0.01 | 0.20 ± 0.02 | 0.20 ± 0.02 |
| slow 1 | 1 | $A_3$ | 0.01 ± 0.01 | 0.03 ± 0.01 | 0.01 ± 0.01 | 0.01 ± 0.01 | 0.03 ± 0.01 | 0.02 ± 0.01 | 0.01 ± 0.01 | 0.01 ± 0.01 |
| | 1 | $t_3$ (s) | 1.03 ± 0.29 | 0.94 ± 0.10 | 1.11 ± 0.18 | 1.15 ± 0.18 | 1.06 ± 0.13 | 1.23 ± 0.27 | 1.00 ± 0.23 | 1.17 ± 0.24 |
| | 2 | $A_3$ | 0.01 ± 0.01 | 0.03 ± 0.02 | 0.01 ± 0.01 | 0.02 ± 0.01 | 0.01 ± 0.01 | 0.00 ± 0.01 | 0.02 ± 0.01 | 0.01 ± 0.01 |
| | 2 | $t_3$ (s) | 0.96 ± 0.42 | 0.78 ± 0.23 | 1.04 ± 0.19 | 1.15 ± 0.12 | 1.31 ± 0.25 | 2.51 ± 1.21 | 0.90 ± 0.29 | 2.03 ± 0.57 |
| slow 2 | 1 | $A_4$ | 0.02 ± 0.01 | 0.02 ± 0.01 | 0.01 ± 0.01 | 0.01 ± 0.01 | 0.01 ± 0.01 | 0.01 ± 0.01 | 0.01 ± 0.01 | 0.01 ± 0.01 |
| | 1 | $t_4$ (s) | 20.9 ± 1.4 | 21.0 ± 1.4 | 25.96 ± 3.01 | 23.8 ± 2.1 | 27.3 ± 4.0 | 20.1 ± 1.9 | 22.3 ± 2.0 | 22.5 ± 1.9 |
| | 2 | $A_4$ | 0.01 ± 0.01 | 0.01 ± 0.01 | 0.00 ± 0.01 | 0.01 ± 0.01 | 0.01 ± 0.01 | 0.00 ± 0.01 | 0.01 ± 0.01 | 0.02 ± 0.01 |
| | 2 | $t_4$ (s) | 18.7 ± 2.5 | 15.5 ± 2.0 | 21.8 ± 3.0 | 14.0 ± 1.5 | 23.2 ± 4.8 | 26.0 ± 11.6 | 21.8 ± 2.7 | 24.2 ± 5.1 |
| fit quality | 1 | $R^2$ | 0.99993 | 0.99994 | 0.99995 | 0.99996 | 0.99994 | 0.99993 | 0.99997 | 0.99995 |
| | 2 | $R^2$ | 0.99997 | 0.99989 | 0.99998 | 0.99997 | 0.99994 | 0.99997 | 0.99985 | 0.99984 |

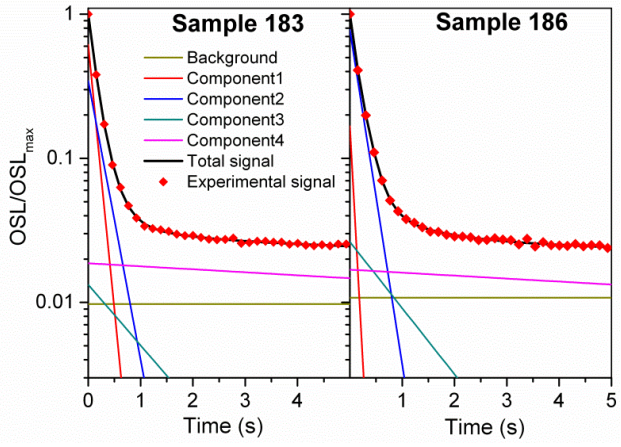


**Fig. 8.** *Examples of CW-OSL curve decomposition into four components for two aliquots of different samples, 183 and 186. Focusing on the intensity relation between the fast and medium components, only the beginning of the curves is presented. The fitting was realized for the entire measurement time range (40 s).*

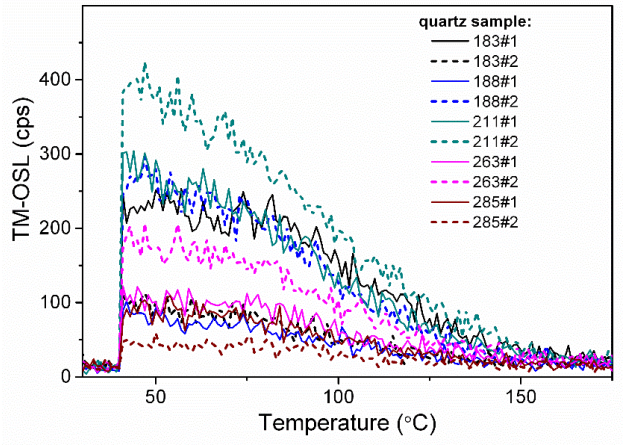


**Fig. 9.** *Natural TM-OSL signal obtained with 620 nm for a few of investigated samples. For each sample a pair of aliquots is shown. The heating rate was 1 Ks$^{-1}$ and the photon flux density 5.3·10$^{17}$ cm$^{-2}$s$^{-1}$. The results illustrate the significant variability in the samples of the fast component intensity measured by TM-OSL with red light.*

signal was bleached. It is worth noting the considerable differences between the signal intensity for samples 183 and 188. However, based on this observation, one should not draw general conclusions about these samples. Another selection of aliquots could indicate other samples with the more remarkable differences in the TM-OSL signal from the fast component.

It is interesting to show how effectively the fast component is isolated from the slower ones through TM-OSL measurement with red diodes. The TM-OSL measurements with various stimulation wavelengths showed that after the fast component was removed by the light with 620 nm, the wavelength of 540/ 530 nm is needed to generate a TM-OSL signal for the OSL component having the next largest OCS in quartz – the medium component (Palczewski and Chruścińska, 2019). **Fig. 10** illustrates this OSL signal behaviour for a reference quartz sample FB (Kreutzer *et al.*, 2017). The results of five TM-OSL measurements taken consecutively after one irradiation (300 Gy) are presented. First, TM-OSL was repeated twice with a stimulation wavelength of 620 nm. Then a TM-OSL measurement was performed with a stimulation wavelength of 580 nm. Finally, TM-OSL was repeated twice with a stimulation wavelength of 530 nm.

As can be seen, the TM-OSL curve with 580 nm has an intensity hardly distinguishable from the background, which proves that the fast OSL component was bleached entirely by the two first TM-OSL runs. **Fig. 10b** presents the result of switching on the diode emitting with a wavelength of 530 nm. Here a curve with significant intensity can be registered. Schmidt *et al.* (2022) demonstrated that the observed luminescence corresponds to the medium OSL component. The described experiment proves that the TM-OSL measurement with 620 nm isolates the fast component from the medium component. At the same time, the curves in **Fig. 10** show that the TM-OSL measurement provides a deeper insight into the nature of the OSL signal than the CW-OSL measurement used in dating so far.

**Fig. 10b**, next to the TM-OSL curve obtained with 530 nm after the fast component bleaching, shows the repetition of the same stimulation directly after measuring the first curve with 530 nm. Characteristic is the change of shape of the TM-OSL curve with 530 nm in the second run

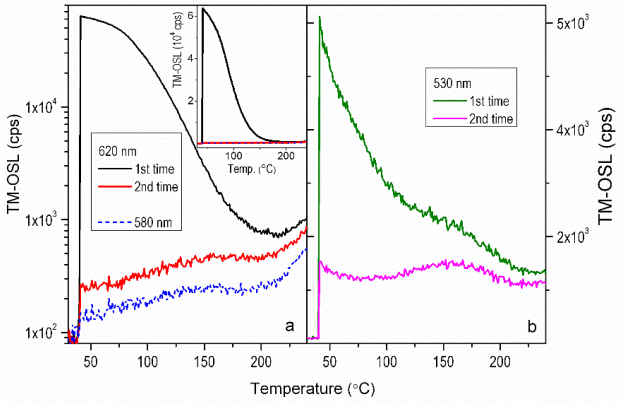


**Fig. 10.** *TM-OSL curves for sample FB measured one after the other with indicated wavelengths 620 nm and 580 nm (a), and next 530 nm (b) after a single excitation with the dose of 300 Gy and preheat to 260 °C. Each optical stimulation was carried out during heating from 40 °C to 240 °C with a rate of 1 K s$^{-1}$ and a photon flux density of 5.3×10$^{17}$ cm$^{-2}$ s$^{-1}$ for 620 nm, 3.9×10$^{16}$ cm$^{-2}$ s$^{-1}$ for 580 nm and 1.7×10$^{17}$ cm$^{-2}$ s$^{-1}$ for 530 nm. The slow heating and the maximal photon flux density achievable for each LED module were used for an effective optical emptying with a particular wavelength before the next wavelength was used. The experiment shows how high a difference in wavelength should be applied to efficiently stimulate the next OSL component after emptying the fast component. From part b, one can also see that the signal measured with 530 nm is complex as its shape changes when repeating the TM-OSL measurement with 530 nm.*

of the experiment. This is the most straightforward proof that the signal observed in the TM-OSL measurement with a wavelength of 530 nm after removing the fast component is composed of at least two slower OSL components. Therefore, attempts to determine the stability of this signal may not bring reproducible results in different samples.

When the stability of the medium component over time is not precisely known, and there are some indications that it is not as stable as the fast component, one should take particular care to avoid the influence of this component on the dating result. Experience so far shows that it is difficult to do this routinely by data analysis. It is much easier to do this at the experimental stage. The SAR TM-OSL using the wavelength of 620 nm provides this.

## 4. Discussion

### 4.1 ED precision

For these tests, samples were selected for which the standard measurements using the SAR BLSL protocol did not bring satisfactory results in terms of the repeatability of ED determined for individual sample aliquots. The reasons for the spread of ED values for individual aliquots of a sample may be manifold. Apart from the inhomogeneous bleaching of sample grains before depositing a layer, one should consider variations in the composition of aliquots in terms of the luminescence properties of individual grains. The ED spread is caused by variations in total luminescence intensities and the relative contributions of individual components in the OSL of the individual grains. This is because each component has its own unique dose-response and quenching rate. Variability in the local concentration of radionuclides (microdosimetry problems) and the post-depositional layers' mixing can also cause ED spread. In the case of the older samples (183, 186, 211, 263, 275), the reason for a significant scatter of the measured ED values may be first of all the insufficient bleaching of the slower OSL components in grains. These samples are derived from fluvial or fluvioglacial sediments. Although geologists have identified them as undergoing processes ensuring the grains' exposition to sunlight prior to sediment formation, such a way of grain transport may not provide sufficient bleaching, particularly of the OSL components slower than the fast component.

The evident reduction in the ED spread in the SAR TM-OSL protocol supports the conjecture that the ED spread in the SAR BLSL results is at least partially related to incomplete bleaching. That is because the measurement of the isolated fast component excludes the specific causes of the ED spread, as a rule. All the factors generating spread mentioned above affect each of the OSL components. However, OSL bleaching stands out from the rest. Bleaching is a factor that differentiates the individual OSL components because the optical cross-section which defines the given component directly determines the rate of optical bleaching.

For sediment, the signal of which has not been zeroed during the transport of grains, the different response of the individual OSL components to bleaching is the cause of the ED spread. That is especially the case for samples whose fast component does not dominate the overall signal sufficiently enough to allow ignoring the contribution of the others. When the slower components have a significant share in total OSL, the ED depends on the contribution of the individual components to the signal used to determine it. This dependence is known and is a basis for a test of sufficient sample bleaching, examining the shape of the CW-OSL decay using the so-called De (t)-plot (e.g Huntley *et al.*, 1985; Perkins and Rhodes, 1994; Bailey 2000, 2003; Steffen *et al.*, 2009). The De (t)-plot was even proposed to be used for ED estimation in samples whose OSL has a significant participation of medium component (Li and Li, 2006).

The contribution of the individual components to the total signal also varies from aliquot to aliquot in the signal used in SAR BLSL to derive the ED (the initial part of CW-OSL curve). It fluctuates due to differences in the concentration of defects responsible for defined components in individual grains and in the composition of grains that make up aliquots. Thus, changes in ED, which are observed when the De (t)-plot is created, also appear as differences in EDs of individual aliquots when one uses the initial part of the CW-OSL curve to derive the ED in the SAR BLSL protocol. Those fluctuations determine the contribution of the incomplete OSL bleaching to the ED spread. As they only occur when the signal measured in SAR BLSL is complex, the isolation of the fast component eliminates this spread constituent and improves ED precision. The improvement becomes more noticeable when there are larger differences in the bleaching of OSL components and greater fluctuations in the proportion of these components in the signal of different aliquots. Since the precision improvement is determined by the two independent factors, the degree of bleaching of individual components and their share in the total OSL, it is not easy to estimate the significance of any of these factors by comparing the scatter sizes obtained in both protocols.

At this point, one should note that the scatter of the EDs determined with the use of the fast component isolated by TM-OSL still includes spread originating from unequal bleaching of grains unless the bleaching was sufficient to zeroing the fast component in all grains.

The mechanism for improving the accuracy of the ED determination in SAR TM-OSL protocol against that obtained by SAR BLSL, which was discussed above, is reflected in the results presented here. Looking at the ED values for individual aliquots in **Fig. 5**, one can see that the difference of the ED spread between SAR BLSL and SAR TM-OSL protocol vary from sample to sample.

As mentioned in **Subsection 3.2**, the application of the new protocol did not improve the ED precision obtained for the younger aeolian sediments (**Fig. 5**). The ED confidence interval calculated for both protocols in the case of

sample 188, differ barely noticeable. The participation of the medium component in OSL of this sample is not negligible (see **Subsection 3.4**). Hence, in line with previous considerations, the bleaching before deposition probably led to OSL zeroing. Interestingly, for two others aeolian samples, 284 and 285, the ED scatter in SAR BLSL protocol is lower than this obtained by protocol SAR TM-OSL. For young sediments, the more significant ED scatter may be caused by the low intensity of the fast component in TM-OSL measurement. Improving the precision of small EDs in the SAR TM-OSL protocol can be achieved by using a stronger source of stimulation light.

For samples 183 and 263, in turn, most ED values for individual aliquots estimated by SAR BLSL protocol agree with the values resulting from SAR TM-OSL protocol. A part of the ED values obtained by the SAR BLSL protocol for several aliquots differ significantly from the rest of the results, and this makes the ED spread greater than that obtained by SAR TM-OSL protocol. In the SAR TM-OSL results, some ED values stand out from the rest, although in much smaller numbers. Based on consistent ED values for individual aliquots obtained from both protocols, it appears that the ED spread constituent resulting from mixing different components in SAR BLSL measurements is less significant in sample 183 and 263 compared to other possible factors, including insufficient bleaching of the grains. Therefore, the SAR TM-OSL does not significantly improve precision for samples 183 and 263, unlike samples 275 or 186.The proportion of ED scatter caused by the composite signal measured in the SAR BLSL was more critical for the latter samples. Using the TM-OSL reduces the standard deviation by 61% (sample 186) and 72% (sample 275).

### 4.2 Cases of untypical TM-OSL curves in SAR TM-OSL protocol

It is worth taking a closer look at the shapes of the curves obtained during the SAR TM-OSL procedure. **Fig. 11** shows examples of TM-OSL measured for aliquots of samples 183 and 263, whose ED results are, respectively, significantly higher and smaller than the mean ED (**Figs. 11a-11c**) and an example of a TM-OSL curve that led to a result close to the mean ED value (**Fig. 11d**). It turns out that not all curves are alike. They look different for the aliquots whose EDs significantly differ from the mean ED. Their TM-OSL curves do not follow the shape of curves measured when the ED of an aliquot is close to the mean ED.

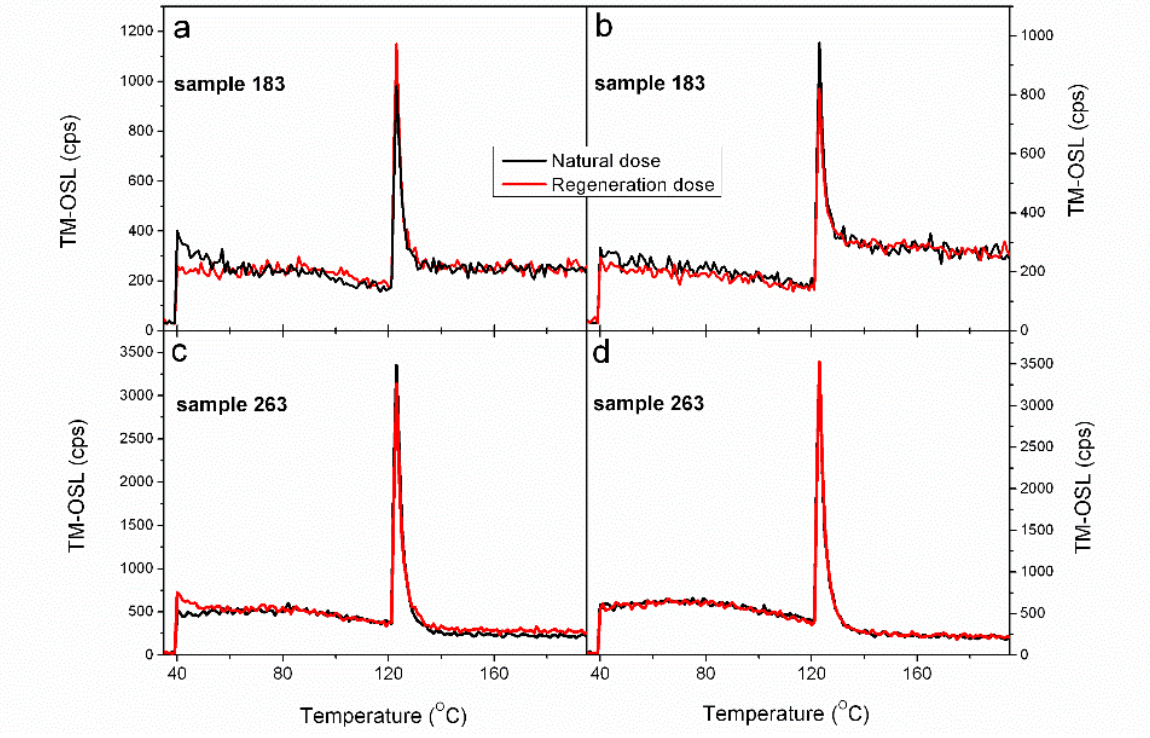


**Fig. 11.** *The heterogeneity of grain features in the sample results in various types of TM-OSL curves inconsistencies observed in SAR TM-OSL protocol. Examples of natural and regenerated TM-OSL curves obtained in protocol SAR TM-OSL for aliquots of samples 183 (a, b) and 263 (c, d) whose ED results differ from the mean ED (a-c) and lead to a result close to the mean ED value (d). In cases (a) and (c), the fast decay is observed at the beginning of the TM-OSL curves. Such decay is not observed in TM-OSL measurements with the same parameters for pure quartz. Case (b) represents the curve, which proves the very high proportion of the slow components in the OSL signal of the aliquot. The curve in part (d) looks like the usual TM-OSL result for quartz of the checked purity. Among curves after the regenerative dose for a given aliquot, those with the intensity most similar to the natural signal were selected.*

So far, for the majority of aliquots of all investigated samples, the curves obtained in procedure SAR TM-OSL were similar to those presented in **Fig. 11d**. Such shapes are also obtained for the calibration quartz and other quartz for which the sample purity tests were performed (reference sample FB and MR, Schmidt *et al.*, 2022). The irregularity of the TM-OSL curve measured for the fast component with wavelength 620 nm, which can be observed in **Fig. 11a** and **11c**, is a fast decay in the initial part of the curve. As mentioned in **Subsection 3.1**, the investigation of single grains being the source of the TM-OSL curve with such deviation from the usual shape identified them as not quartz. In general, it should be recognized that such a rapid decay at the beginning proves that the measured signal TM-OSL does not come only from the fast component in quartz. Therefore, care should be taken when including aliquots with such irregular signals in ED calculations. When one assumes that the irregular shape of the TM-OSL curve can be the basis for eliminating an aliquot and one recalculates the ED, the latter is further improved. For sample 183 (omitted three aliquots with the highest ED), it is 28.8 ± 5 Gy; for sample 263 (omitted one aliquot having the highest ED), 66 ± 12 Gy.

For sample 275, SAR TM-OSL results for individual aliquots did not contain values as significantly different from the mean ED as for samples 183 and 263. TM-OSL curves of the aliquots accepted for the age calculation were regular. No curve deformations similar to those shown in **Fig. 11a** and **11c** were observed. Therefore, one may suppose that the significant ED spread in the SAR BLSL protocol results is not due to the luminescence heterogeneity of grains. Such a situation is probable for samples 183 and 263 whose TM-OSL curves were unusual (see **Fig. 11a** and **11c**). In the TM-OSL signal of sample 275, various grain properties are not manifested.

### 4.3. Samples with signal close to saturation

The results obtained for samples whose signal is evidently close to the saturation are worth a separate discussion. Here, we can deal with either sediment whose age exceeds the OSL dating limit or a younger one that was most likely not bleached at all or to such a small extent, that the natural OSL signal remains in the saturation range, making the age estimation completely impossible. It is not easy to settle which situation is the case here. Interestingly, in the case of sample 211, the individual aliquot EDs obtained from the SAR TM-OSL protocol fall within the middle of the dose range indicated by the spread of EDs in the SAR BLSL protocol. However, for sample 186, the EDs are mostly concentrated at the lower end of this range. One might assume that the described difference in EDs obtained by the protocol SAR TM-OSL for both samples is due to at least a partial bleaching of the fast OSL component in sample 186 during the grains' transport. However, it does not necessarily have to be this way. Such an effect may be due to a different saturation level of the fast OSL component in relation to the saturation level for the total OSL signal measured with blue LEDs. Therefore, the ED value obtained by SAR TM-OSL protocol cannot be treated as an approximation of the upper age limit of the sediment layer.

The fast component signal may be saturated here due to the lack of resetting, as can be in the case of the rest of the OSL signal. The growth curves obtained for individual aliquots of samples 186 and 211 indicate this. The ED for the fast component may be lower than for the total OSL when the saturation level of the fast component in the sample is lower than the saturation level of the sum of all the components. The saturation level depends on many factors (Chen *et al.*, 2020, Pawlak and Chruścińska, 2025), including the concentration of centres active in the processes accompanying luminescence. Both the external conditions and the concentration of the centres can vary significantly from sample to sample. Hence it is difficult to expect that the relation of the saturation level of the fast components to this level for the total OSL signal is fixed in various samples. The manifestation of this seems to be the different results of applying the SAR TM-OSL protocol for samples 186 and 211. In both samples, the fast component is most likely saturated. However, the relation of its saturation level to the saturation level of the total OSL signal, which is the sum of many components, appears to be different.

Such an eventuality draws attention to another advantage of the SAR TM-OSL protocol, apart from using a signal that is effectively reset during grain transport. The recently highlighted problem of OSL dating is the limited ED range for which the natural dose response curve (DRC) conforms to the laboratory curve (Chapot *et al.*, 2012; Timar-Gabor and Wintle, 2013; Timar-Gabor *et al.*, 2015; Peng *et al.*, 2022). While the primary reason for the DRCs discrepancy coming to mind is the enormous difference in the dose rate used in the laboratory and nature, it is interesting to note that this may not be the only cause. The recent study by Peng *et al.* (2022) shows that the range of the compatibility of the natural and laboratory generated DRC can be widened using the sensitivity-corrected multiple-aliquot regenerative-dose (MAR) protocol with the blue light stimulation (Zhou and Shackleton, 2001; Lowick and Preusser, 2011). This example shows that the problem of non-compliance of curves lies, at least in part, in the method of measuring an OSL signal and in that one determines the DRCs for the complex OSL signal in quartz. In the light of the recently presented simulations, the level of OSL saturation depends on the competition of different paths of charge relaxation during excitation (Chen *et al.*, 2020). The latter depends, among others, on the mutual relation between concentrations of the individual defects in the crystal. Therefore, it is essential to establish both the natural and laboratory dose response curves (DRC) for a specific OSL component, rather than for the sum of components whose contributions to the total signal vary with

the dose. The results obtained from samples within the saturation range of equivalent doses (EDs) strongly suggest the necessity for this approach.

## 5. Conclusions

The equivalent dose is the basis for determining the age of the sediment sample in OSL dating. The presented study compares the results of the measurement of the equivalent dose by the SAR protocol commonly used in OSL dating based on quartz up to now and two other recently developed protocols using light with a much longer wavelength than the SAR protocol for stimulation. The SAR protocol with the optical stimulation using 620 nm in CW-OSL measurement, although it led to correct preliminary test results using a calibration quartz sample, in the here conducted test of sediment sample dating, mostly does not bring acceptable results. Usually, the recuperation or recycling tests eliminate a large proportion of the aliquots. Apart from a different wavelength of light, the second newly tested, SAR TM-OSL protocol, also uses a new stimulation method which consists of illuminating the sample while heating it linearly. The adequately performed SAR TM-OSL using 620 nm allows calculating the OSL age using exclusively the fast OSL component which is most effectively bleached during the sediment formation. The presented research shows the following potential of the SAR TM-OSL protocol:

1) SAR TM-OSL protocol leads mostly to ages consistent within uncertainties with the SAR BLSL ages. For samples characterized in SAR BLSL by the wide distribution of ED results for individual aliquots, the precision of EDs obtained by SAR TM-OSL protocol is mostly better than these obtained by SAR BLSL.
2) Using an isolated fast component in SAR TM-OSL protocol prevents participation in the signal used for the age determination of components with other thermal and dose-response characteristics. Their presence cannot be identified in the SAR BLSL protocol without additional signal analysis and may influence the OSL age.
3) The TM-OSL curves' shape helps verify the signal of the investigated sample in terms of the similarity to the TM-OSL signal of pure quartz that was used to establish the parameters of the SAR TM-OSL protocol. One can decide about excluding the irregular aliquots from the measurements.

The advantages of the SAR TM-OSL protocol require confirmation in studies on a much larger group of samples of more diverse origins. However, the effect of the selective using the fast component on the precision of OSL dating results is unquestionable. Thus it is worth conducting such more comprehensive studies. Especially when conducting TM-OSL measurements does not require a significant technical change in the readers used in dating or a prolonged time of measurements.

## Acknowledgements

This work has been done thanks to the help of the Centre for Modern Interdisciplinary Technologies, Nicolaus Copernicus University in Torun, ul. Wilenska 4, 87-100 Torun, Poland (e-mail: icnt@umk.pl) and has been partially financed by the grant of the National Science Centre, Poland, No. 2018/31/B/ST10/03917.

## References

Aitken MJ, 1998. Introduction to optical dating: the dating of Quaternary sediments by the use of photon-stimulated luminescence. Oxford University Press, Oxford, DOI 10.1093/oso/9780198540922.001.0001.

Bailey RM, 2000. The interpretation of quartz optically stimulated luminescence equivalent dose versus time plots. *Radiation Measurements* 32: 129–140, DOI 10.1016/S1350-4487(99)00256-5.

Bailey RM, 2003. Paper II: The interpretation of measurement-time-dependent single-aliquot equivalent-dose estimates using predictions from a simple empirical model. *Radiation Measurements* 37: 685–691, DOI 10.1016/S1350-4487(03)00079-9.

Bailey RM, 2010. Direct measurement of the fast component of quartz optically stimulated luminescence and implications for the accuracy of optical dating. *Quaternary Geochronology* 5: 559–568, DOI 10.1016/j.quageo.2009.10.003.

Bailey RM, Smith BJ and Rhodes EJ, 1997. Partial bleaching and the decay form characteristics of quartz OSL. Radiation Measurements 27: 123–136, DOI 10.1016/S1350-4487(96)00157-6.

Bailey RM, Yukihara EG and McKeever SWS, 2011. Separation of quartz optically stimulated luminescence components using green (525 nm) stimulation. *Radiation Measurements* 46: 643–648, DOI 10.1016/j.radmeas.2011.06.005.

Bourgoin J and Lannoo M, 1983. Point defects in semiconductors II, Berlin: Springer–Verlag, DOI 10.1007/978-3-642-81832-5.

Bulur E, Bøtter-Jensen L and Murray AS, 2000. Optically stimulated luminescence from quartz measured using the linear modulation technique. *Radiation Measurements* 32(5–6): 407–411, DOI 10.1016/S1350-4487(00)00115-3.

Cunningham AC and Wallinga J, 2009. Optically stimulated luminescence dating of young quartz using the fast component. *Radiation Measurements* 44: 423–428, DOI 10.1016/j.radmeas.2009.02.014.

Cunningham AC and Wallinga J, 2010. Selection of integration time intervals for quartz OSL decay curves. *Quaternary Geochronology* 5: 657–666, DOI 10.1016/j.quageo.2010.08.004.

Chapot MS, Roberts HM, Duller GAT and Lai ZP, 2012. A comparison of natural- and laboratory-generated dose response curves for quartz optically stimulated luminescence signals from Chinese Loess. *Radiation Measurements* 47(11–12): 1045–1052, DOI 10.1016/j.radmeas.2012.09.001.

Chen R, Lawless JL and Pagonis V, 2020. Competition between long time excitation and fading of thermoluminescence (TL) and optically stimulated luminescence (OSL). *Radiation Measurements* 136: 106422, DOI 10.1016/j.radmeas.2020.106422.

Chruścińska A and Kijek N, 2016. Thermally modulated optically stimulated luminescence (TM–OSL) as a tool of trap parameter analysis.

*Journal of Luminescence* 174: 42–48, DOI 10.1016/j.jlumin.2016.01.012.

Chruścińska A, Palczewski P, Rerek T, Biernacka M and Lefrais Y, 2021. Measurement of the paleodose in luminescence dating using the TM-OSL of quartz. *Measurement* 167: 108448, DOI 10.1016/j.measurement.2020.108448.

Chruścińska A and Palczewski P, 2020. OSL characteristics: theory and experiments. *Radiation Protection Dosimetry* 192: 266–293, DOI 10.1093/rpd/ncaa205.

Chruścińska A, Palczewski P and Rerek T, 2020. Slow OSL component in quartz separated by TM-OSL method. *Radiation Measurements* 134: 106316, DOI 10.1016/j.radmeas.2020.106316.

Chruścińska A and Szramowski A, 2018a. Thermally modulated optically stimulated luminescence (TM-OSL) of quartz. *Journal of Luminescence* 195: 435–440, DOI 10.1016/j.jlumin.2017.12.004.

Chruścińska A and Szramowski A, 2018b. Thermally modulated OSL related to the fast component of the OSL signal in quartz. *Radiation Measurements* 120: 20–25, DOI 10.1016/j.radmeas.2018.05.011.

Durcan JA and Duller GAT, 2011. The fast ratio: a rapid measure for testing the dominance of the fast component in the initial OSL signal from quartz. *Radiation Measurements* 46: 1065–1072, DOI 10.1016/j.radmeas.2011.07.016.

Fan A, Li S-H and Li B, 2009. Characteristics of quartz infrared stimulated luminescence (IRSL) at elevated temperatures. *Radiation Measurements* 44: 434–438, DOI 10.1016/j.radmeas.2009.02.019.

Galbraith RF, Roberts RG, Laslett GM, Yoshida H and Olley JM, 1999. Optical dating of single and multiple grains of quartz from Jinmium rock shelter, northern Australia: Part 1, experimental design and statistical models. *Archaeometry* 41: 339–364, DOI 10.1111/j.1475-454.1999.tb00987.x.

Hansen V, Murray AS, Buylaert J-P, Yeo E-Y and Thomsen KJ, 2015. A new irradiated quartz for beta source calibration. *Radiation Measurements* 81: 123–127, DOI 10.1016/j.radmeas.2015.02.017.

Huntley DJ, Godfrey-Smith DI and Thewalt ML, 1985. Optical dating of sediments. *Nature* 313: 105–107, DOI 10.1038/313105a0.

Jain M, Murray AS and Bøtter-Jensen L, 2003. Characterisation of blue-light stimulated luminescence components in different quartz samples: implications for dose measurement. *Radiation Measurements* 37(4–5), 441–449, DOI 10.1016/S1350-4487(03)00052-0.

Kitis G, Polymeris GS and Kiyak NG, 2007. Component-resolved thermal stability and recuperation study of the LM-OSL curves of four sedimentary quartz samples. *Radiation Measurements* 42(8): 1273–1279, DOI 10.1016/j.radmeas.2007.05.050.

Kreutzer S, Friedrich J, Sanderson D, Adamiec G, Chruścińska A, Fasoli M, Martini M, Polymeris G, Burbidge C and Schmidt C, 2017. Les sables de Fontainebleau: a natural quartz reference sample and its characterisation. *Ancient TL* 35(2): 21–37. DOI 10.26034/la.atl.2017.515.

Li B and Li S-H, 2006. Comparison of De estimates using the fast component and the medium component of quartz OSL. *Radiation Measurements* 41: 125–136, DOI 10.1016/j.radmeas.2005.06.037.

Lowick SE and Preusser F, 2011. Investigating age underestimation in the high dose region of optically stimulated luminescence using fine grain quartz. *Quaternary Geochronology* 6(1): 33–41, DOI 10.1016/j.quageo.2010.08.001.

Murray AS and Roberts RG, 1998. Measurement of the equivalent dose in quartz using a regenerative-dose single-aliquot protocol. *Radiation Measurements* 29: 503–515, DOI 10.1016/S1350-4487(98)00044-4.

Murray AS and Wintle AG, 1998. Factors controlling the shape of the OSL decay curve in quartz. *Radiation Measurements* 29: 65–79, DOI 10.1016/S1350-4487(97)00207-2.

Murray AS and Wintle AG, 2000. Luminescence dating of quartz using an improved single-aliquot regenerative-dose protocol. *Radiation Measurements* 32: 57–73, DOI 10.1016/S1350-4487(99)00253-X.

Murray AS and Wintle AG, 2003. The single aliquot regenerative dose protocol: potential for improvements in reliability. *Radiation Measurements* 37: 377–381, DOI 10.1016/S1350-4487(03)00053-2.

Noras JM, 1980. Photoionization and phonon coupling. *Journal of Physics C-Solid State Physics* 13(25): 4779, DOI 10.1088/0022-3719/13/25/019.

Palczewski P and Chruścińska A, 2019. Different components of the quartz OSL signal resolved by the TM-OSL method. *Radiation Measurements* 121: 32–36, DOI 10.1016/j.radmeas.2018.12.005.

Pawlak N and Chruścińska A, 2025. Reliability of trap-filling parameters read from OSL dose-response curves measured by procedures with sensitivity correction. *Radiation Physics and Chemistry* 227: 1–13, DOI 10.1016/j.radphyschem.2024.112365.

Peng J and Wang XL, 2020. On the production of the medium component in quartz OSL: Experiments and simulations. *Radiation Measurements* 138: 106448, DOI 10.1016/j.radmeas.2020.106448.

Peng J, Wang X and Adamiec G, 2022. The build-up of the laboratory-generated dose-response curve and underestimation of equivalent dose for quartz OSL in the high dose region: A critical modelling study. *Quaternary Geochronology* 67: 101231, DOI 10.1016/j.quageo.2021.101231.

Perkins NK and Rhodes EJ, 1994. Optical dating of fluvial sediments from Tattershall, UK. *Quaternary Geochronology* 13: 517–520, DOI 10.1016/0277-3791(94)90069-8.

Schmidt Ch, Chruścińska A, Fasoli M, Biernacka M, Kreutzer S, Polymeris GS, Sanderson DCW, Cresswell A, Adamiec G and Martini M, 2022. A systematic multi-technique comparison of luminescence characteristics of two reference quartz samples. *Journal of Luminescence* 250: 119070, DOI 10.1016/j.jlumin.2022.119070.

Singarayer JS and Bailey RM, 2003. Further investigations of the quartz optically stimulated luminescence components using linear modulation. *Radiation Measurements* 37(4–5): 451–458, DOI 10.1016/S1350-4487(03)00062-3.

Singarayer JS and Bailey RM, 2004. Component-resolved bleaching spectra of quartz optically stimulated luminescence: preliminary results and implications for dating. *Radiation Measurements* 38: 111–118, DOI 10.1016/S1350-4487(03)00250-6.

Skuja L, 2000. Optical properties of defects in silica. In: Pacchioni,G.,Skuja,L. and Griscom,D.L. (Ed.), Defects in $SiO_2$ and related dielectrics: Science and Technology. Kluwer Academic, Boston. 73–116, DOI 10.1007/978-94-010-0944-7_3.

Smith BW, Aitken MJ, Rhodes EJ, Robinson PD and Geldard DM, 1986. Optical dating: Methodological aspects. *Radiation Protection Dosimetry* 17: 229–233, DOI 10.1093/rpd/17.1-4.229.

Smith BW and Rhodes EJ, 1994. Charge movements in quartz and their relevance to optical dating. *Radiation Measurements* 23(2–3): 329–333, DOI 10.1016/1350-4487(94)90060-4.

Spooner NA, 1994. On the optical dating signal from quartz. *Radiation Measurements* 23: 593–600, DOI 10.1016/1350-4487(94)90105-8.

Steffen D, Preusser F and Schlunegger F, 2009. OSL quartz age underestimation due to unstable signal components. *Quaternary Geochronology* 4: 353–362, DOI 10.1016/j.quageo.2009.05.015.

Tamura T, Sawai Y and Ito K, 2015. OSL dating of the AD 869 Jogan tsunami deposit, northeastern Japan. *Quaternary Geochronology* 30: 294–298, DOI 10.1016/j.quageo.2015.06.001.

Timar-Gabor A, Constantin D, Buylaert JP, Jain M, Murray AS and Wintle AG, 2015. Fundamental investigations of natural and laboratory generated SAR dose response curves for quartz OSL in the high dose range. *Radiation Measurements* 81: 150–156, DOI 10.1016/j.radmeas.2015.01.013.

Timar-Gabor A and Wintle AG, 2013. On natural and laboratory generated dose response curves for quartz of different grain sizes from Romanian loess. *Quaternary Geochronology* 18: 34–40, DOI 10.1016/j.quageo.2013.08.001.

Wang XL, Du JH, Adamiec G and Wintle AG, 2015. The origin of the medium OSL component in West Australian quartz. *Journal of Luminescence* 159: 147–157, DOI 10.1016/j.jlumin.2014.11.003.

Wintle AG and Murray AS, 1998. Towards the development of a preheat procedure for OSL dating of quartz. *Radiation Measurements* 29: 81–94, DOI 10.1016/S1350-4487(97)00228-X.

Wintle AG and Murray AS, 1999. Luminescence sensitivity changes in quartz. *Radiation Measurements* 30: 107–118, DOI 10.1016/S1350-4487(98)00096-1.

Wintle AG and Murray AS, 2000. Quartz OSL: effects of thermal treatment and their relevance to laboratory dating procedures. *Radiation Measurements* 32: 387–400, DOI 10.1016/S1350-4487(00)00057-3.

Wintle AG and Murray AS, 2006. A review of quartz optically stimulated luminescence characteristics and their relevance in single-aliquot regeneration dating protocols. *Radiation Measurements* 41: 369–391, DOI 10.1016/j.radmeas.2005.11.001.

Vandenberghe DAG, Jain M and Murray AS, 2008. A note on spurious luminescence from silicone oil. *Ancient TL*. 26: 29–32, DOI 10.26034/la.atl.2008.420.

Zhou LP and Shackleton NJ, 2001. Photon-stimulated luminescence of quartz from loess and 658 effects of sensitivity change on palaeodose determination. *Quaternary Science Reviews* 20(5–9): 853–857, DOI 10.1016/S0277-3791(00)00024-X.